Effect of carbon-coated Al$_2$O$_3$ powder on structure and properties of low-carbon MgO-C refractory composites

Xiangyu Tian[1], Guoqi Liu[1,*], Xinlian Shang[1], Hongxia Li[1,*], Xinfu Wang[1,*], Wengang Yang[1], Yongqiang Chen[2]

[1]*Sinosteel Luoyang Institute of Refractories Research Co. Ltd., State Key Laboratory of Advanced Refractories, Luoyang, Henan, 471039 China*
[2]*School of Materials Science and Engineering, Zhengzhou University, Zhengzhou, Henan 450001 China*

Abstract

In this study, low-carbon MgO-C refractory composites with addition of uncoated (UA) and carbon-coated Al$_2$O$_3$ (CCA) powders were prepared. The effect of heat-treatment temperature on apparent porosity, cold modulus of rupture and thermal expansion was investigated. The results indicated that the CCA was present in the form of porous agglomerates of 400–800 µm in diameter in MgO-C matrix. The formation of spinel started at 1100 °C and 1250 °C in UA-MgO-C and CCA-MgO-C specimens, respectively. In the specimen CCA-MgO-C, cyclic spinel was formed on the outer layer of CCA agglomerates, and the dense spinel layer hindered the diffusion of Mg(g) to the interior of the agglomerates, resulting in alumina residues at 1550 °C. The specimen CCA-MgO-C showed better mechanical properties and reduced porosity. Additionally, the average coefficient of thermal expansion of CCA-MgO-C was significantly lower than that of UA-MgO-C. Thus, CCA powder could improve the volume stability of the low-carbon MgO-C refractory composites.

Keywords: low-carbon MgO-C composites, carbon-coated Al$_2$O$_3$ powder, spinel reaction, volume stability

I. Introduction

Graphite, which has high thermal conductivity, low thermal expansion, low elasticity modulus and low wettability by molten slag, is one of the important main ingredients for making carbon-containing refractories [1]. However, when the carbon content is too high, the refractories bring more carbon than necessary into the molten metal and also lead to the loss of thermal energy through the furnace walls and have poor oxidation resistance [2]. MgO-C refractories have been widely used as the linings of converters, electric arc furnaces, steel ladles and RH vacuum degassers due to its excellent corrosion resistance and thermal shock resistance [1–4]. Nevertheless, their carbon content as high as 12–18 wt.% causes problem as it is relatively high. Some efforts have been made to modify the refractory proper-

ties by simply reducing the carbon dosage [5–7], however, it was found that the thermal shock resistance of the refractories decreased greatly along with poor corrosion resistance and wettability [8–10].

Recently, several researchers have paid more attention to overcoming the mechanical and thermal properties of low-carbon MgO-C composites by adopting nanotechnology [11,12], using more efficient additives [13], binding agents [14] and carbon source [15]. *In situ* spinel formation is accompanied by volumetric expansion, which leads to a significant reduction in pore volume and improves the oxidation resistance and thermal shock resistance of low-carbon MgO-C refractories [16–19]. The current adjustment of the spinel reaction is generally used to add metal [14,20,21] or metal oxide [22–24], change MgO, Al$_2$O$_3$ particles size and content [25], or control the reaction atmosphere [26]. Zhu *et al.* [20] found on the basis of microstructural observations and compositional analysis that the addition of metallic Al and low graphite content played essential roles in the formation of the hollow MgO-rich spinel whiskers. Zhang [27] reported that an *in situ* catalysed-growth

* Corresponding authors:
tel: +86 0379 64206330, e-mail: *liugq@lirrc.com.* (G. Liu)
tel: +86 0379 64205801, e-mail: *lihongx0622@126.com* (H. Li)
tel: +86 0379 64205907, e-mail: *wangxf@lirrc.com* (X. Wang)

technique was developed to form large quantities of oxide nanofibers and/or carbon nanotubes in carbon-containing refractories with a transition metal catalyst via a catalysed vapour deposition process. Zhang *et al.* [28] also found that Al reacted with surrounding carbon and/or N_2 to form Al_4C_3 and/or AlN at high temperatures. The formed Al_4C_3 further reacts with N_2 to form AlN whiskers and/or with CO to form Al_2O_3, which could further lead to the formation of $MgAl_2O_4$ particles through the reaction with MgO. Bavand-Vandchali *et al.* [29] indicated that the formation of in situ spinel via reaction of reactive Al_2O_3 and MgO fine grain started at 1000 °C and accomplished at 1300 °C. Al_2O_3 and MgO usually produced MA-spinel by solid-phase interdiffusion [30], but the contact of MgO and Al_2O_3 was hindered by the presence of carbon in carbonaceous material. At the same time, the formation mechanism of MA-spinel had undergone great changes in reducing atmosphere [31]. MgO could react with solid C [32,33] to form Mg(g). Al_2O_3 could also generate $Al_2O(g)$, Al(g) and Al(l), etc. [34,35]. Mg(g) could react with $Al_2O_3(s)$, $Al_2O(g)$, Al(g) and Al(l) to form fibrous [36] or cyclic [31] spinel by gas-solid reaction (V-S) and gas-liquid-solid (V-L-S) reaction. The formed spinel is deposited on the surface of MgO particles or Al_2O_3 particles.

However, the mechanical properties of composites decrease significantly with the increase of spinel content due to the thermal expansion mismatch [25]. This reaction also produces microcracks by the rapid thermal expansion which aggravates the penetration of slag. The refractories for continuous casting system, which are prepared as composite structure of MgO-C and Al_2O_3-C refractories, undergo spinel reaction at the interface between the two materials. This can result in the problems of volumetric expansion and volumetric instability. For example, it may cause breakage and continuous casting accident such as stopper rod head fracture. Therefore, the regulation of *in situ* reaction of spinel is an important technology which affects the service behaviour of carbon-containing refractories.

In this paper, for the first time carbon-coated Al_2O_3 powder was introduced into MgO-C refractories to separate the contact between MgO and Al_2O_3. Thus, spinel could only be formed by gas phase reaction, which effectively controls spinel reaction rate and ensured the volume stability of the materials. Also the influence of *in situ* spinel on the microstructure, phase composition, mechanical and thermal properties is reported.

II. Experimental procedures

2.1. Preparation of the specimens

Fused magnesia (with three different particle sizes: ≤ 1 mm, ≤ 0.15 mm, ≤ 0.088 mm, 97.38 wt.% MgO, Dashiqiao City Tianyu Mining Co., Ltd., China), calcined alumina (d_{50} = 10 μm, 99.70 wt.% Al_2O_3, Zhengzhou Yuli Industry Co., Ltd., China), flake graphite (≤ 0.088 mm, 97.58 wt.% fixed carbon, Qingdao Zhongkai Graphite Co., Ltd., China) and carbon black (≤ 250 nm, 98.03 wt.% fixed carbon, Evonik Industries AG, China) were used as raw materials. Thermosetting phenolic resin (Liquid, 42 wt.% of carbon yield, SQ Group, China) was used as the binder.

Two specimens were prepared according to Table 1. For the first one (CCA-MgO-C), alumina and carbon black were pre-mixed by high-speed mixer (R02, Maschienfabrik Gustav Erich) for 30 min (1000 rpm) to obtain CCA powder. Part of resin was added to CCA powder in order to coat the carbon black on the alumina surface. Finally, CCA powder and resin were mixed for 10 min and dried at 60 °C for 12 h. In the specimen CCA-MgO-C, fused magnesia, flake graphite, remaining resin and CCA agglomerates were mixed for 30 min. In the specimen UA-MgO-C, all raw materials were mixed directly by high-speed mixer for about 70 min. The compositions of the two specimens were exactly the same. After kneading, bar shaped specimen (25 mm × 25 mm × 150 mm) were compacted under a pressure of 120 MPa and then cured at 180 °C for 12 h. Finally, all the specimens were heat-treated at a heating rate of 1 °C/min to 950, 1100, 1250, 1400 and 1550 °C for 5 h in a corundum saggar filled with carbon black, respectively.

2.2. Characterization of the specimens

The microstructure and phase composition of the specimen heat-treated at different temperatures were analysed by scanning electron microscope (SEM, EVO-18, ZEISS, DE) coupled with energy dispersive X-ray spectroscopy (EDS, X-Max 50, Oxford, UK) and X-ray diffraction (XRD, X'Pert Pro, Philips, Eindhoven, Ni, Cu K_α radiation), respectively. The bulk density

Table 1. Batch composition

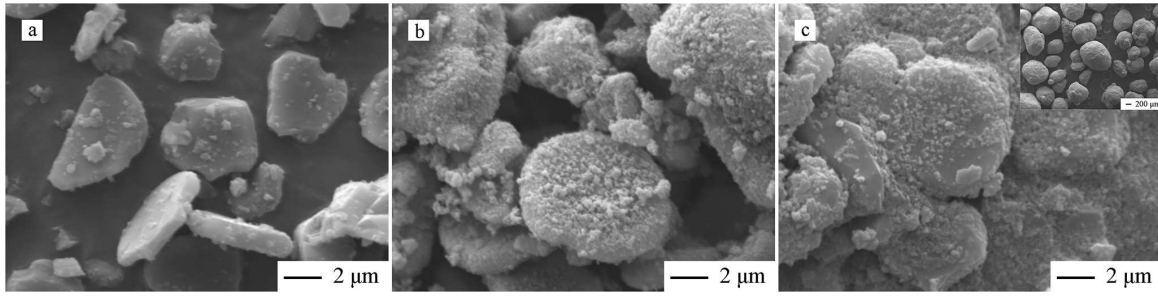| Raw materials		CCA-MgO-C [wt.%]	UA-MgO-C [wt.%]
Fused magnesia	≤ 1 mm	50	50
	≤ 0.150 mm	20	20
	≤ 0.088 mm	15	15
Flake graphite	≤ 0.088 mm	3	3
CCA powder	400–800 μm	12	
Calcined alumina	d_{50} = 10 μm		10
Carbon black	≤ 250 nm		2
Resin	liquid	+6	+6

Figure 1. SEM images of: a) calcined alumina powder, b) CCA powder before adding resin and c) CCA powder after adding resin

(BD) and apparent porosity (AP) were determined by the Archimedes method in kerosene. The cold modulus of rupture (CMOR, WHY-200, Lirr, China) was measured by three-point bending test. The thermal shock resistance (in a reducing atmosphere) of the specimens heat-treated at 950 and 1100 °C was evaluated with the method of water quenching. The heat-treated specimens were heated at 1100 °C for 10 min in a reducing atmosphere and then placed into flowing water at room temperature for 5 min. The specimens were dried, and then the values of their residual cold modulus of rupture (CMOR$_{st}$) were determined after one thermal shock cycle.

The thermal expansions (from room temperature to 1550 °C) of the specimens heat-treated at 950 °C were measured by rod-type indirect method. The thermal expansion percent (ρ) and coefficient of thermal expansion (α) can be calculated based on the following equation:

$$\rho = \frac{(L_t - L_0) + A_K(t)}{L_0} \cdot 100 \tag{1}$$

$$\alpha = \frac{\rho}{(t - t_0) \cdot 100} \tag{2}$$

where L_0 is the length of the specimen at room temperature, L_t is the length of the specimen at experimental temperature, $A_K(t)$ is the instrument calibration value at experimental temperature, t_0 is the room temperature and t is experimental temperature.

III. Results and discussion

3.1. Phase composition and microstructure

Figure 1 shows the typical scanning electron microscopy image of the calcined alumina powder and obtained CCA powder before and after adding resin. It was found that the calcined alumina powder has hexagonal morphology and the carbon black was evenly coated on the surface of the alumina before adding resin. The resin made the CCA powder agglomerate and immobilized the carbon black on the surface of the alumina. The average size of the CCA agglomerates was 400–800 μm.

Figure 2a shows the XRD patterns of the specimen UA-MgO-C heat-treated at different temperatures. The presence of MA-spinel phase was detected from 1100 °C and its peaks intensity increased steadily with heat-treatment temperature. Spinel, periclase and graphite were identified as dominant crystalline phases after 1100 °C, while corundum phase content decreased rapidly with increasing temperature and disappeared above 1100 °C. However, the XRD patterns of the specimen CCA-MgO-C (Fig. 2b) show that the peaks of MA-spinel phase did not appear until 1250 °C. Meanwhile, the peak of corundum still existed up to 1550 °C.

Figures 3a and 3b show SEM micrographs of the specimens UA-MgO-C and CCA-MgO-C heat-treated at 950 °C. It can be seen from Fig. 3a that the Al$_2$O$_3$ is uniformly distributed in the matrix and directly in contact with MgO in the specimen UA-MgO-C. However,
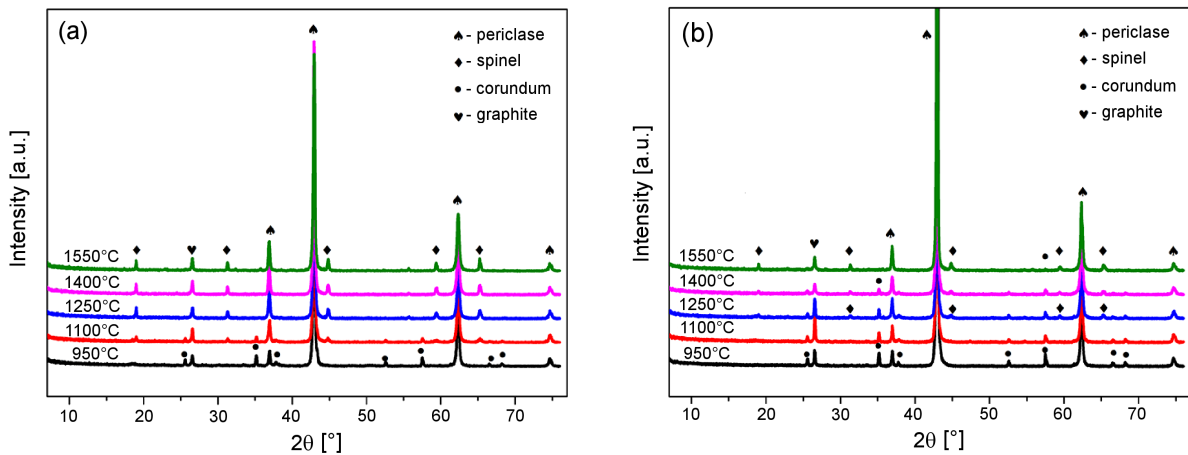

Figure 2. XRD patterns of: a) UA-MgO-C and b) CCA-MgO-C heat-treated at different temperatures
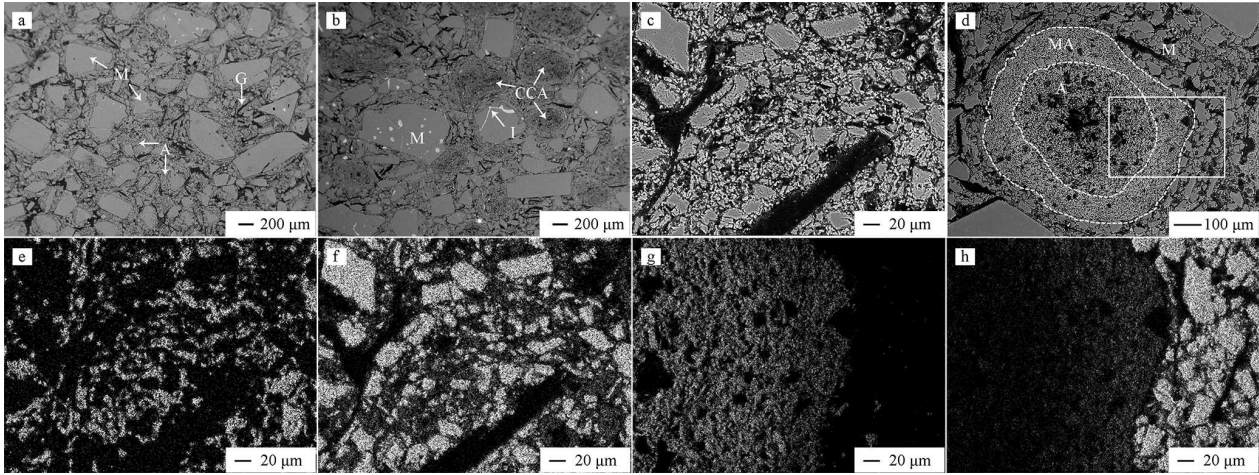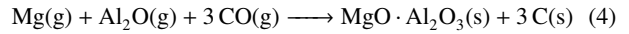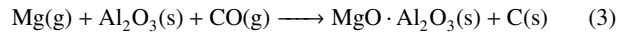
Figure 3. SEM images of: a) UA-MgO-C heat-treated at 950 °C, b) CCA-MgO-C heat-treated at 950 °C, c) UA-MgO-C heat-treated at 1550 °C, d) CCA-MgO-C heat-treated at 1550 °C. The distribution of elements: e) Al in Fig. 3c, f) Mg in Fig. 3c, g) Al element in the solid line of Fig. 3d, h) Mg in the solid line of Fig. 3d

in the specimen CCA-MgO-C (Fig. 3b) Al_2O_3 exists in the form of CCA agglomerates and the interface was observable between CCA agglomerates and MgO. Particularly, Fig. 3b reveals a hollow space existing in the interior of CCA agglomerates. During the heat treatment, these Al_2O_3 particles started to react with surrounding MgO grains to form primary spinel. Al_2O_3 was completely converted to spinel and uniformly distributed in the matrix at 1550 °C in the specimen UA-MgO-C (Figs. 3c,e,f). The CCA agglomerates present two layers textures at 1550 °C. The outer layer was denser, but the inner layer was looser. There was still a clear interface between agglomerates and magnesia. According to the XRD results (Fig. 2b) and the distribution of the elements (Figs. 3g,h), it can be concluded that the dense layer was spinel and the loose layer was alumina. It could be concluded from the comparison of Figs. 3g,h that the Mg element was present in the interior of the CCA agglomerates, while the Al element could not diffuse outwards. However, the spinel formation was controlled by counter-diffusion of Mg^{2+} and Al^{3+} ions in the solid phase reaction [30]. Therefore, the formation of dense spinel was probably due to the gas phase reactions (3) and (4). Mg(g) diffused to the alumina surface

through the interstices within the aggregate and reacted with Al_2O_3(s) and Al_2O(g) to form spinel. The volumetric expansion caused by the spinel reaction led to the densification of the outer layer of CCA agglomerates and hindered the further diffusion of Mg(g) to the interior, eventually resulting in incomplete reaction [31].

$$Mg(g) + Al_2O_3(s) + CO(g) \longrightarrow MgO \cdot Al_2O_3(s) + C(s) \quad (3)$$

$$Mg(g) + Al_2O(g) + 3\,CO(g) \longrightarrow MgO \cdot Al_2O_3(s) + 3\,C(s) \quad (4)$$

3.2. Mechanical properties

The apparent porosity and cold modulus rupture of the specimens CCA-MgO-C and UA-MgO-C heat-treated at different temperatures (950, 1100, 1250, 1400 and 1550 °C) are presented in Fig. 4. As shown in Fig. 4a, the AP of the specimen UA-MgO-C increased steadily with heat-treatment temperature. However, the AP of the specimen CCA-MgO-C increased from 950 to 1250 °C, and decreased from 1250 to 1550 °C. Meanwhile, the AP of the specimen UA-MgO-C was obviously higher than that of CCA-MgO-C. For example, the AP of the specimens CCA-MgO-C and UA-MgO-
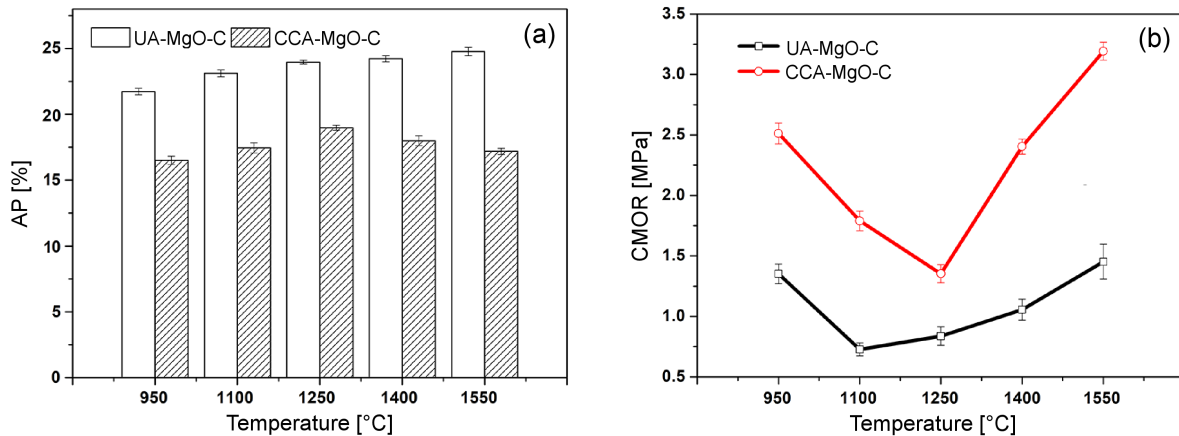

Figure 4. Properties of specimens CCA-MgO-C and UA-MgO-C: a) apparent porosity (AP) and b) cold modulus rupture (CMOR)

C at 1100 °C were 17% and 23%, respectively. During heat-treatment process, the phenolic resin decomposed and porous pyrolytic carbon remained [36], resulting in an increase in the porosity of the specimen. In the specimen CCA-MgO-C, the CCA agglomerates provided a more reasonable particle size distribution for the material to reduce the porosity of the material at low temperatures. With temperature rising, the spinel generated in the porous surface of CCA agglomerates and blocked the pores, so that the apparent porosity of the material was reduced.

As shown in Fig. 4b, the CMOR of the specimen UA-MgO-C clearly decreased with the increase of temperature from 950 to 1100 °C and then increased simultaneously with the temperature up to 1550 °C. However, in the specimen CCA-MgO-C, the lowest point of CMOR appeared at 1250 °C, and the CMOR at different temperatures was significantly higher than that of the specimen UA-MgO-C. The CMOR of all the specimens was mainly affected by the morphology of residual carbon after heat treatment and the development of spinel. Before the CMOR of the specimen reached its lowest point, the reticular carbon produced by the resin pyrolysis in the specimen was gradually destroyed with the increase of temperature, and then the CMOR was decreased. With the temperature increase, the spinel reaction occurred, and the ceramic began to form in the specimen, resulting in a gradual increase in strength. The thermal shock behaviour of the specimens heat-treated at 950 and 1100 °C was expressed by the residual CMOR after one cycle of the thermal shock test (named as CMORst). No matter what the heat-treatment temperature is, the specimen CCA-MgO-C exhibited higher residual CMOR compared to the specimen UA-MgO-C (as shown in Table 2). Thus, CCA powder had a positive effect on the thermal shock resistance of low-carbon MgO-C refractory specimens.

The improvements in the mechanical properties were greatly associated with the changes in the microstructures of the specimens [14]. The porosity of CCA-MgO-C was significantly lower than that of UA-MgO-C. Therefore, the structure of CCA-MgO-C was more dense, which promoted the CMOR of CCA-MgO-C.

3.3. Thermal expansion

Figure 5 shows the thermal expansion percent (ρ) of the specimens UA-MgO-C and CCA-MgO-C heat-treated at 950 °C from room temperature (RT) to 1550 °C. Owing to the thermal expansion space provided by the high porosity, the ρ of CCA-MgO-C was slightly higher than that of UA-MgO-C from RT to 800 °C. The ρ of the specimens CCA-MgO-C and UA-MgO-C was 0.72% from RT to 800 °C. When the temperature was higher than 800 °C, the ρ of CCA-MgO-C was lower than that of UA-MgO-C. The average coefficient of thermal expansions (α) of CCA-MgO-C and UA-MgO-C were 10.4×10^{-6} K^{-1} and 10.9×10^{-6} K^{-1}, respectively (as shown in Table 3). With temperature rising, the average coefficient of thermal expansion of CCA-MgO-C did not change significantly. However, for the specimen UA-MgO-C a sharp expansion from 1175 to 1375 °C appeared. The α and ρ of UA-MgO-C increased to 14.6×10^{-6} K^{-1}1 and 1.95% at 1375 °C, respectively. However, the temperature of sharp expansion was higher than that of the spinel reaction which was 1100 °C (as shown in Fig. 2a). This may be due to the difference in holding time. In the test of thermal expansion, the specimen was not withheld at any temperature.
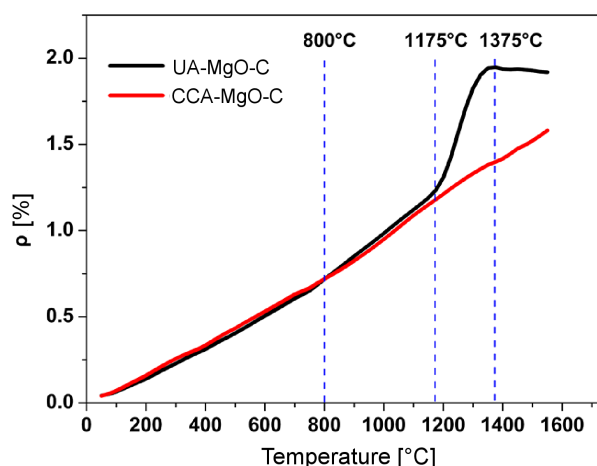

Figure 5. Thermal expansion percent (ρ) of specimens UA-MgO-C and CCA-MgO-C heat-treated at 950 °C

Table 2. CMOR change of specimens CCA-MgO-C and UA-MgO-C heat-treated at 950 and 1100 °C after one cycle of thermal shock test

	CCA-MgO-C		UA-MgO-C	
Heat-treatment temperature [°C]	950	1100	950	1100
CMOR [MPa]	2.51	1.79	1.35	0.73
CMOR$_{st}$ [MPa]	2.06	1.23	0.87	0.48
Residual strength ratio [%]	81.94	79.89	64.01	65.99

Table 3. The average coefficient of thermal expansion (α) of specimens UA-MgO-C and CCA-MgO-C in different temperature ranges

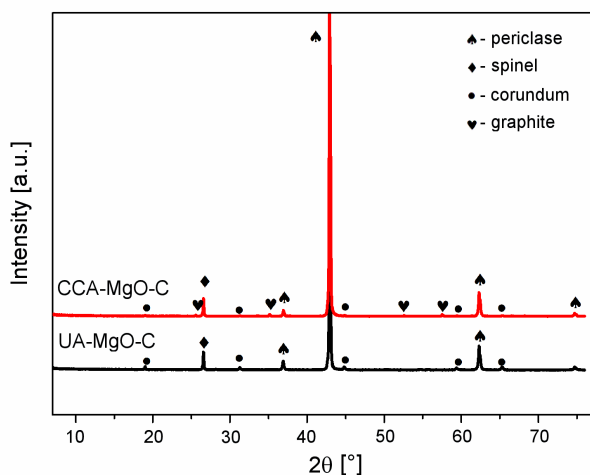| Sample	α [10^{-6} K^{-1}]			
	RT to 800 °C	RT to 1175 °C	RT to 1375 °C	RT to 1550 °C
CCA-MgO-C	9.4	10.4	10.4	10.5
UA-MgO-C	9.4	10.9	14.6	12.8

Figure 6. XRD patterns of the specimens after thermal expansion test

Thus, the volumetric expansion caused by the spinel reaction emerged as hysteresis. When the spinel reaction was completed in the specimen UA-MgO-C, sintering phenomenon occurred, which made the specimen shrink from 1375 to 1550 °C.

Figure 6 shows the XRD patterns of the specimen after thermal expansion test. Periclase, graphite, and spinel phases exist in the specimen UA-MgO-C, and the specimen CCA-MgO-C also contained corundum phase.

Figure 7 shows the SEM images of the specimens after thermal expansion test. Due to the lack of necessary grain growth time, no regular octahedral spinel grains were found in both specimens. EDS analysis was performed on the hexagonal grains (which was Al_2O_3 before the thermal expansion test) on the surface of the CCA agglomerates. The results showed that the composition of the points 1, 2 and 3 (Fig. 7b, Table 4) were all close to that of the standard MA-spinel. So the spinel was generated on the surface of the CCA agglomerates in the specimen CCA-MgO-C. Some incomplete octahedral grains were found in the matrix of the specimen UA-MgO-C (as shown in Fig. 7d). The EDS results (points 4, 5 and 6, Table 4) showed that these grains were MA-spinel. So the spinel was generated in the matrix of the specimen UA-MgO-C and the crystal growth was better than in the specimen CCA-MgO-C.

In UA-MgO-C the spinel was generated evenly in the matrix. As shown in Fig. 8a, when there were enough pores around the area where spinel was generated, the pores could effectively absorb the expansion effect. However, if the spinel was formed in the region without pores, it would also generate stress on the surround-

Table 4. The relative content of Al_2O_3 and MgO at different points shown in Fig. 7

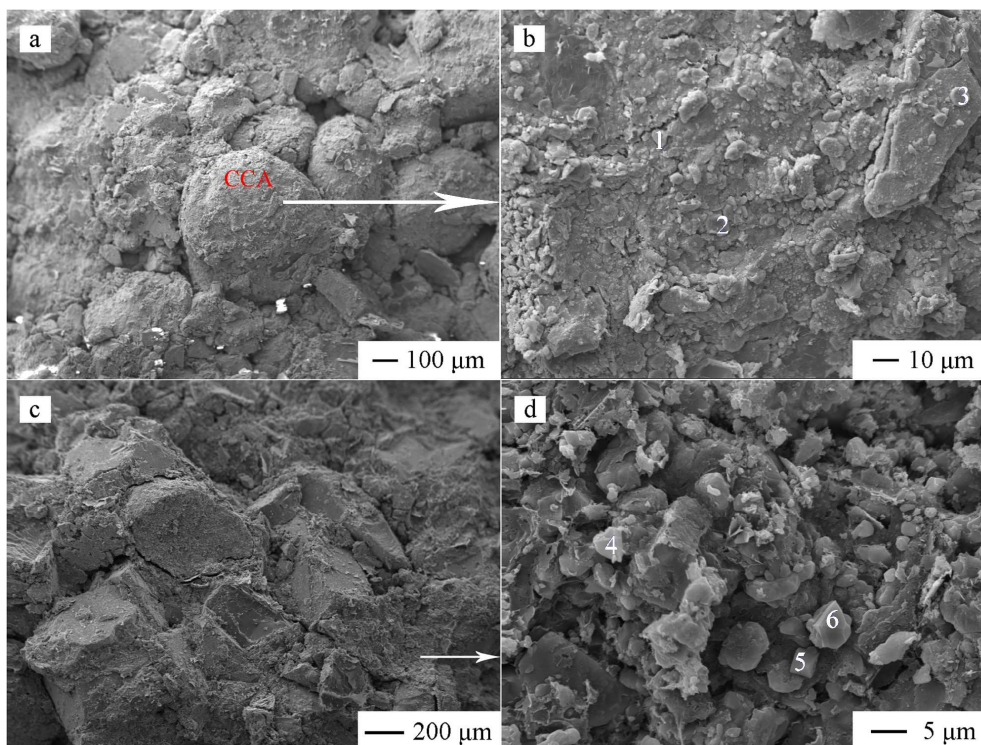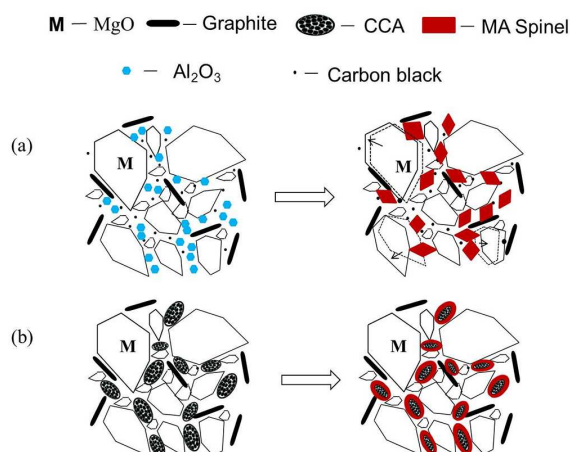|	Relative content [%]						
	standard	1	2	3	4	5	6
Al_2O_3	71.83	73.34	70.85	71.69	71.55	71.33	70.37
MgO	28.17	26.65	29.15	28.31	28.45	28.67	29.62

Figure 7. SEM images of the specimens after thermal expansion test: a) CCA-MgO-C, b) surface of CCA, c) UA-MgO-C and d) matrix of specimen CCA-MgO-C

Figure 8. Effect of spinel reaction on the thermal expansion of different specimens: a) UA-MgO-C and b) CCA-MgO-C

ing MgO grains, resulting in the movement of MgO and then the specimen would expand. The microstructure of CCA-MgO-C confirms existence of a hollow space in the interior and on the surface of CCA agglomerates. Mg(g) diffused to the alumina surface through the interstices within the aggregate and reacted with Al_2O_3(s) to form spinel. In comparison with the specimen UA-MgO-C, the spinel was generated on the porous surface of agglomerates, which could effectively absorb the volumetric expansion caused by the spinel reaction (as shown in Fig. 8b). So the specimen CCA-MgO-C could not produce a sharp expansion phenomenon.

IV. Conclusions

The low-carbon MgO-C refractories with the carbon coated alumina powder (CCA) addition were prepared. The effects of heat-treatment temperature on the phase composition, microstructure and properties were also carried out. The main conclusions of the study are the following:

1. The average particle diameter of the CCA powder fixed by the resin was within the range of 400–800 μm.
2. In specimen CCA-MgO-C, a dense ring-like spinel was formed on the periphery of the agglomerates by gas phase reaction at 1250 °C. In specimen UA-MgO-C, the *in situ* spinel appeared in the matrix at 1100 °C. The mechanical properties of CCA-MgO-C were significantly higher than that of UA-MgO-C.
3. The specimen CCA-MgO-C did not present the sharp expansion phenomenon, which is caused by the spinel reaction. Thus, carbon-coated Al_2O_3 powder could ensure the volume stability of the low-carbon MgO-C refractory composites.

References

1. E.M.M. Emad, "Carbon based refractories", *J. Ceram. Soc. Jpn.*, **112** (2004) 517–532.
2. M. Bag, S. Adak, R. Sarkar, "Nano carbon containing MgO-C refractory: effect of graphite content", *Ceram. Int.*, **38** (2012) 4909–4914.
3. S. Hayashi, H. Takahashi, A. Watanabe, A. Osaka, Y. Miura, "Dependence of mechanical properties of MgO-C bricks on graphite content", *J. Ceram. Soc. Jpn.*, **102** (2010) 23–28.
4. I.K. Bae, M.C. Kim, D.H. Chung, M.D. Shin, Y.H. Seo, "The improvement of MgO-C bricks toughness for RH snorkels", *Proceedings of the UNITECR'05 Congress*, November, Orlando, USA, 2005.
5. B. Liu, J.L. Sun, G.S. Tang, K.Q. Liu, L. Li, Y.F. Liu, "Effect of nanometer carbon black on performance of low-carbon MgO-C composites", *J. Iron Steel Res. Int.*, **17** (2010) 75–78.
6. L. Musante, L.F. Martorello, P.G. Galliano, A.L. Cavalieri, A.G. Tomba Martinez, "Mechanical behaviour of MgO-C refractory bricks evaluated by stress-strain curves", *Ceram. Int.*, **38** (2012) 4035–4047.
7. S. Mahato, S.K. Pratihar, S.K. Behera, S.K. Behera, "Fabrication and properties of MgO-C refractories improved with expanded graphite", *Ceram. Int.*, **40** (2014) 16535–16542.
8. L. Li, *Study on Properties Modification and Microstructure of Low-Carbon Magnesia-Carbon Composite*, University of Science and Technology Beijing, 2005 (in Chinese).
9. T. Zhu, Y. Li, S. Sang, Z. Xie, "Mechanical behavior and thermal shock resistance of MgO-C refractories: Influence of graphite content", *Ceram. Int.*, **43** (2017) 7177–7183.
10. Z. Liu, J. Yu, X. Yang, E. Jin, L. Yuan, "Oxidation resistance and wetting behavior of MgO-C refractories: Effect of carbon content", *Materials*, **11** (2018) 883.
11. T. Zhu, Y. Li, S. Jin, S. Sang, N. Liao, "Catalytic formation of one-dimensional nanocarbon and MgO whiskers in low carbon MgO-C refractories", *Ceram. Int.*, **41** (2015) 3541–3548.
12. T. Zhu, Y. Li, S. Sang, S. Jin, Y. Li, L. Zhao, X. Liang, "Effect of nanocarbon sources on microstructure and mechanical properties of MgO-C refractories", *Ceram. Int.*, **40** (2014) 4333–4340.
13. T. Wang, A. Yamaguchi, "Oxidation protection of MgO-C refractories by means of $Al_8B_4C_7$", *J. Am. Ceram. Soc.*, **84** (2001) 577–582.
14. G. Wei, B. Zhu, X. Li, Z. Ma, "Microstructure and mechanical properties of low-carbon MgO-C refractories bonded by an Fe nanosheet-modified phenol resin", *Ceram. Int.*, **41** (2015) 1553–1566.
15. T. Bahtli, D.Y. Hopa, V.M. Bostanci, S.Y. Yasti, "Thermal conductivity of MgO-C refractory ceramics: Effects of pyrolytic liquid and pyrolytic carbon black obtained from waste tire", *Ceram. Int.*, **44** (2018) 13848–13851.
16. F.C. Duncan, *Expansion During the Formation of the Magnesium Aluminate Spinel ($MgAl_2O_4$) from its Basic Oxide MgO and Al_2O_3 Powders*, University of Alabama, USA, 2004.
17. E.Y. Sako, M.A.L. Braulio, E. Zinngrebe, S.R. van der

Laan, V.C. Pandolfelli, "Fundamentals and applications on in situ spinel formation mechanisms in Al_2O_3-MgO refractory castables", *Ceram. Int.*, **38** (2012) 2243–2251.

18. M.A.L. Braulio, L.R.M. Bittencourt, V.C. Pandolfelli, "Magnesia grain size effect on in situ spinel refractory castables", *J. Eur. Ceram. Soc.*, **28** (2008) 2845–2852.

19. M. Deepak., S. Debasish, "Effect of in situ spinel seeding on synthesis of MgO-rich $MgAl_2O_4$ composite", *J. Mater. Sci.*, **42** (2007) 7286–7293.

20. T. Zhu, Y. Li, S. Sang, S. Jin, H. Wang, "Formation of hollow MgO-rich spinel whiskers in low carbon MgO-C refractories with Al additives", *J. Eur. Ceram. Soc.*, **34** (2014) 4425–4432.

21. J.W. Lee, J.G. Duh, "High-temperature MgO-C-Al refractories-metal reactions in high aluminum content alloy steels", *J. Mater. Res.*, **18** (2003) 1950–1959.

22. A. Ghosh, S.K. Das, J.R. Biswas, H.S. Tripathi, G. Banerjee, "The effect of ZnO addition on the densification and properties of magnesium aluminate spinel", *Ceram. Int.*, **20** (2000) 605–608.

23. W. Yuan, C. Deng, H. Zhu, "Effects of TiO_2 addition on the expansion behavior of alumina–magnesia refractory castables", *Mater. Chem. Phys.*, **162** (2015) 724–733.

24. R. Sarkar, G. Bannerjee, "Effect of addition of TiO_2 on reaction sintered MgO-Al_2O_3 spinels", *J. Eur. Ceram. Soc.*, **20** (2000) 2133–2141.

25. C. Aksel, F.L. Riley, "Effect of the particle size distribution of spinel on the mechanical properties and thermal shock performance of MgO-spinel composites", *J. Eur. Ceram. Soc.*, **23** (2003) 3079–3087.

26. A.D. Mazzoni, M.A. Sainz, A. Caballero, E.F. Aglietti, "Formation and sintering of spinels ($MgAl_2O_4$) in reducing atmospheres", *Mater. Chem. Phys.*, **78** (2003) 30–37.

27. S. Zhang, "Next generation carbon-containing refractory composites", *Adv. Sci. Technol.*, **45** (2006) 2246–2253.

28. S. Zhang, N.J. Marriott, W.E. Lee, "Thermochemistry and microstructures of MgO-C refractories containing various antioxidants", *J. Eur. Ceram. Soc.*, **21** (2001) 1037–1047.

29. M. Bavand-Vandchali, F. Golestani-Fard, H. Sarpoolaky, H.R. Rezaie, C.G. Aneziris, "The influence of in situ spinel formation on microstructure and phase evolution of MgO-C refractories", *J. Eur. Ceram. Soc.*, **28** (2008) 563–569.

30. M. Rigaud, S. Palco, N. Wang, "Spinel formation in the MgO-Al_2O_3 system relation to basic castables", pp. 384–394 in *Proceedings of the UNITECR'95*, Kyoto, Japan, 1995.

31. M. Bavand-Vandchali, H. Sarpoolaky, F. Golestani-Fard, H.R. Rezaie, "Atmosphere and carbon effects on microstructure and phase analysis of *in situ* spinel formation in MgO-C refractories matrix", *Ceram. Int.*, **35** (2009) 861–868.

32. M. Faghihi-Sani, A. Yamaguchi, "Oxidation kinetics of MgO-C refractory bricks", *Ceram. Int.*, **28** (2002) 835–839.

33. L. Musante, V. Muñoz, M.H. Labadie, A.G. Tomba Martinez, "High temperature mechanical behavior of Al_2O_3-MgO-C refractories for steelmaking use", *Ceram. Int.*, **37** (2011) 1473–1483.

34. M. Emmel, C.G. Aneziris, F. Sponza, S. Dudczig, P. Colombo, "*In situ* spinel formation in Al_2O_3-MgO-C filter materials for steel melt filtration", *Ceram. Int.*, **40** (2014) 13507–13513.

35. P. Lefort, M. Billy, "Mechanism of AIN formation through the carbothermal reduction of Al_2O_3 in a flowing N_2 atmosphere", *J. Am. Ceram. Soc.*, **76** (1993) 2295–2299.

36. Y. Liu, X. Jing, "Pyrolysis and structure of hyperbranched polyborate modified phenolic resins", *Carbon*, **45** (2007) 1965–1971.